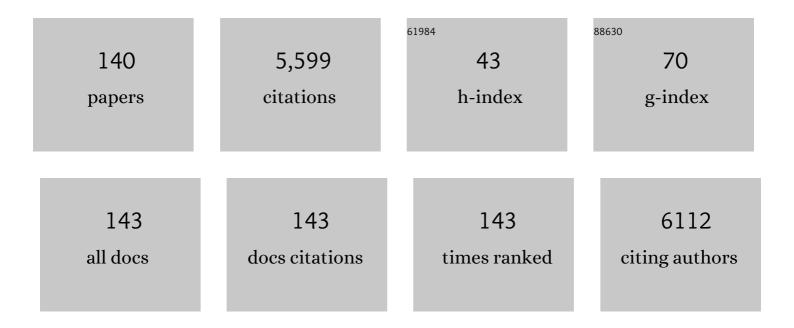
## Mark A Baker

List of Publications by Year in descending order

Source: https://exaly.com/author-pdf/6957350/publications.pdf Version: 2024-02-01



MADE A RAKED

#	Article	IF	CITATIONS
1	XPS investigation of monatomic and cluster argon ion sputtering of tantalum pentoxide. Applied Surface Science, 2017, 405, 79-87.	6.1	191
2	The initiation of pitting corrosion at MnS inclusions. Corrosion Science, 1993, 34, 667-682.	6.6	185
3	Identification of gene products present in Triton X-100 soluble and insoluble fractions of human spermatozoa lysates using LC-MS/MS analysis. Proteomics - Clinical Applications, 2007, 1, 524-532.	1.6	176
4	Identification of SRC as a key PKA-stimulated tyrosine kinase involved in the capacitation-associated hyperactivation of murine spermatozoa. Journal of Cell Science, 2006, 119, 3182-3192.	2.0	170
5	An in depth investigation of deactivation through carbon formation during the biogas dry reforming reaction for Ni supported on modified with CeO2 and La2O3 zirconia catalysts. International Journal of Hydrogen Energy, 2018, 43, 18955-18976.	7.1	165
6	The importance of redox regulated pathways in sperm cell biology. Molecular and Cellular Endocrinology, 2004, 216, 47-54.	3.2	155
7	Reactive oxygen species in spermatozoa: methods for monitoring and significance for the origins of genetic disease and infertility. Reproductive Biology and Endocrinology, 2005, 3, 67.	3.3	152
8	The mouse sperm proteome characterized <b><i>via</i></b> IPG strip prefractionation and LCâ€MS/MS identification. Proteomics, 2008, 8, 1720-1730.	2.2	149
9	Highly selective and stable nickel catalysts supported on ceria promoted with Sm2O3, Pr2O3 and MgO for the CO2 methanation reaction. Applied Catalysis B: Environmental, 2021, 282, 119562.	20.2	149
10	Ni supported on CaO-MgO-Al2O3 as a highly selective and stable catalyst for H2 production via the glycerol steam reforming reaction. International Journal of Hydrogen Energy, 2019, 44, 256-273.	7.1	138
11	Investigating the correlation between deactivation and the carbon deposited on the surface of Ni/Al2O3 and Ni/La2O3-Al2O3 catalysts during the biogas reforming reaction. Applied Surface Science, 2019, 474, 42-56.	6.1	128
12	Localized corrosion of a 2219 aluminium alloy exposed to a 3.5% NaCl solution. Corrosion Science, 2010, 52, 2855-2866.	6.6	121
13	Head and flagella subcompartmental proteomic analysis of human spermatozoa. Proteomics, 2013, 13, 61-74.	2.2	115
14	Carbamazepine degradation using a N-doped TiO 2 coated photocatalytic membrane reactor: Influence of physical parameters. Journal of Hazardous Materials, 2016, 310, 98-107.	12.4	115
15	Identification of post-translational modifications that occur during sperm maturation using difference in two-dimensional gel electrophoresis. Proteomics, 2005, 5, 1003-1012.	2.2	112
16	The rat sperm proteome characterized <b><i>via</i></b> IPG strip prefractionation and LCâ€MS/MS identification. Proteomics, 2008, 8, 2312-2321.	2.2	103
17	Nanoporous activated carbon cloth as a versatile material for hydrogen adsorption, selective gas separation and electrochemical energy storage. Nano Energy, 2017, 40, 49-64.	16.0	101
18	Simple surface treatments to modify protein adsorption and cell attachment properties within a poly(dimethylsiloxane) micro-bioreactor. Surface and Interface Analysis, 2006, 38, 198-201.	1.8	97

#	Article	IF	CITATIONS
19	Ni/Y2O3–ZrO2 catalyst for hydrogen production through the glycerol steam reforming reaction. International Journal of Hydrogen Energy, 2020, 45, 10442-10460.	7.1	85
20	Proteomic insights into the maturation and capacitation of mammalian spermatozoa. Systems Biology in Reproductive Medicine, 2012, 58, 211-217.	2.1	80
21	An "Unlikely―Pair: The Antimicrobial Synergy of Polymyxin B in Combination with the Cystic Fibrosis Transmembrane Conductance Regulator Drugs KALYDECO and ORKAMBI. ACS Infectious Diseases, 2016, 2, 478-488.	3.8	80
22	The initiation of pitting corrosion of stainless steels at oxide inclusions. Corrosion Science, 1992, 33, 1295-1312.	6.6	79
23	Highly selective and stable Ni/La-M (M=Sm, Pr, and Mg)-CeO2 catalysts for CO2 methanation. Journal of CO2 Utilization, 2021, 51, 101618.	6.8	78
24	Highly Stretchable, Directionally Oriented Carbon Nanotube/PDMS Conductive Films with Enhanced Sensitivity as Wearable Strain Sensors. ACS Applied Materials & Interfaces, 2019, 11, 39560-39573.	8.0	75
25	Analysis of proteomic changes associated with sperm capacitation through the combined use of IPGâ€strip preâ€fractionation followed by RP chromatography LCâ€MS/MS analysis. Proteomics, 2010, 10, 482-495.	2.2	72
26	The Relationship between Reaction Temperature and Carbon Deposition on Nickel Catalysts Based on Al2O3, ZrO2 or SiO2 Supports during the Biogas Dry Reforming Reaction. Catalysts, 2019, 9, 676.	3.5	72
27	Design Aspects of Doped CeO <sub>2</sub> for Low-Temperature Catalytic CO Oxidation: Transient Kinetics and DFT Approach. ACS Applied Materials & Interfaces, 2021, 13, 22391-22415.	8.0	70
28	Identification of Cytochrome P450-Reductase as the Enzyme Responsible for NADPH-Dependent Lucigenin and Tetrazolium Salt Reduction in Rat Epididymal Sperm Preparations1. Biology of Reproduction, 2004, 71, 307-318.	2.7	68
29	Impact of water quality on removal of carbamazepine in natural waters by N-doped TiO2 photo-catalytic thin film surfaces. Journal of Hazardous Materials, 2013, 244-245, 463-471.	12.4	67
30	The influence of SiO2 doping on the Ni/ZrO2 supported catalyst for hydrogen production through the glycerol steam reforming reaction. Catalysis Today, 2019, 319, 206-219.	4.4	67
31	Electrodeposited Nanostructured CoFe2O4 for Overall Water Splitting and Supercapacitor Applications. Catalysts, 2019, 9, 176.	3.5	65
32	Effect of operating parameters on the selective catalytic deoxygenation of palm oil to produce renewable diesel over Ni supported on Al2O3, ZrO2 and SiO2 catalysts. Fuel Processing Technology, 2020, 209, 106547.	7.2	65
33	Rapid microwave assisted sol-gel synthesis of CeO2 and CexSm1-xO2 nanoparticle catalysts for CO oxidation. Molecular Catalysis, 2017, 428, 41-55.	2.0	62
34	Nanostructure, mechanical and tribological properties of reactive magnetron sputtered TiCx coatings. Diamond and Related Materials, 2008, 17, 2054-2061.	3.9	61
35	Cu, Sm co-doping effect on the CO oxidation activity of CeO2. A combined experimental and density functional study. Applied Surface Science, 2020, 521, 146305.	6.1	61
36	Nanocomposite hydroxyapatite formation on a Ti–13Nb–13Zr alloy exposed in a MEM cell culture medium and the effect of H2O2 addition. Acta Biomaterialia, 2009, 5, 63-75.	8.3	60

#	Article	IF	CITATIONS
37	The 'omics revolution and our understanding of sperm cell biology. Asian Journal of Andrology, 2011, 13, 6-10.	1.6	56
38	Morphology-dependent electrochemical performance of MnO2 nanostructures on graphene towards efficient capacitive deionization. Electrochimica Acta, 2020, 330, 135202.	5.2	55
39	Identification of Cytochrome-b5 Reductase as the Enzyme Responsible for NADH-Dependent Lucigenin Chemiluminescence in Human Spermatozoa1. Biology of Reproduction, 2005, 73, 334-342.	2.7	54
40	Proteomic insights into spermatozoa: critiques, comments and concerns. Expert Review of Proteomics, 2009, 6, 691-705.	3.0	54
41	Label-Free Quantitation of Phosphopeptide Changes During Rat Sperm Capacitation. Journal of Proteome Research, 2010, 9, 718-729.	3.7	53
42	Phosphorylation and consequent stimulation of the tyrosine kinase c-Abl by PKA in mouse spermatozoa; its implications during capacitation. Developmental Biology, 2009, 333, 57-66.	2.0	49
43	Promoting effect of CaO-MgO mixed oxide on Ni/ $\hat{I}^3$ -Al2O3 catalyst for selective catalytic deoxygenation of palm oil. Renewable Energy, 2020, 162, 1793-1810.	8.9	47
44	From Breast Cancer to Antimicrobial: Combating Extremely Resistant Gram-Negative "Superbugs―Using Novel Combinations of Polymyxin B with Selective Estrogen Receptor Modulators. Microbial Drug Resistance, 2017, 23, 640-650.	2.0	45
45	Nickel Supported on AlCeO3 as a Highly Selective and Stable Catalyst for Hydrogen Production via the Glycerol Steam Reforming Reaction. Catalysts, 2019, 9, 411.	3.5	39
46	Cu-Ce-La-Ox as efficient CO oxidation catalysts: Effect of Cu content. Applied Surface Science, 2020, 505, 144474.	6.1	39
47	Analysis of Phosphopeptide Changes as Spermatozoa Acquire Functional Competence in the Epididymis Demonstrates Changes in the Post-translational Modification of Izumo1. Journal of Proteome Research, 2012, 11, 5252-5264.	3.7	38
48	Hard and superhard TiAlBN coatings deposited by twin electron-beam evaporation. Surface and Coatings Technology, 2007, 201, 6078-6083.	4.8	36
49	Use of Titanium Dioxide To Find Phosphopeptide and Total Protein Changes During Epididymal Sperm Maturation. Journal of Proteome Research, 2011, 10, 1004-1017.	3.7	36
50	A robust inverse analysis method to estimate the local tensile properties of heterogeneous materials from nano-indentation data. International Journal of Mechanical Sciences, 2017, 123, 162-176.	6.7	36
51	Optimizing the oxide support composition in Pr-doped CeO2 towards highly active and selective Ni-based CO2 methanation catalysts. Journal of Energy Chemistry, 2022, 71, 547-561.	12.9	36
52	The influence of an OTS self-assembled monolayer on the wear-resistant properties of polysilicon based MEMS. Surface and Interface Analysis, 2006, 38, 863-867.	1.8	34
53	Ce–Sm– <i>x</i> Cu cost-efficient catalysts for H <sub>2</sub> production through the glycerol steam reforming reaction. Sustainable Energy and Fuels, 2019, 3, 673-691.	4.9	34
54	The nanostructure, wear and corrosion performance of arc-evaporated CrBxNy nanocomposite coatings. Surface and Coatings Technology, 2009, 204, 246-255.	4.8	33

#	Article	IF	CITATIONS
55	Proteomic Characterization of Pig Sperm Anterior Head Plasma Membrane Reveals Roles of Acrosomal Proteins in ZP3 Binding. Journal of Cellular Physiology, 2015, 230, 449-463.	4.1	32
56	N-Doped TiO2-Coated Ceramic Membrane for Carbamazepine Degradation in Different Water Qualities. Nanomaterials, 2017, 7, 206.	4.1	32
57	Structure–Activity Relationships of Daptomycin Lipopeptides. Journal of Medicinal Chemistry, 2020, 63, 13266-13290.	6.4	30
58	Corrosion behaviour of a 2219 aluminium alloy treated with a chromate conversion coating exposed to a 3.5% NaCl solution. Corrosion Science, 2011, 53, 1214-1223.	6.6	28
59	An XPS study of bromine in methanol etching and hydrogen peroxide passivation treatments for cadmium zinc telluride radiation detectors. Applied Surface Science, 2013, 264, 681-686.	6.1	27
60	Effect of Pt nanoparticle decoration on the H2 storage performance of plasma-derived nanoporous graphene. Carbon, 2021, 171, 294-305.	10.3	27
61	A comparison of in situ polishing and ion beam sputtering as surface preparation methods for XPS analysis of PVD coatings. Thin Solid Films, 2000, 377-378, 473-477.	1.8	26
62	Development of the signalling pathways associated with sperm capacitation during epididymal maturation. Molecular Reproduction and Development, 2003, 64, 446-457.	2.0	26
63	Needle grass array of nanostructured nickel cobalt sulfide electrode for clean energy generation. Surface and Coatings Technology, 2018, 354, 306-312.	4.8	26
64	A comparative study of Ni catalysts supported on Al2O3, MgO–CaO–Al2O3 and La2O3–Al2O3 for the dry reforming of ethane. International Journal of Hydrogen Energy, 2022, 47, 5337-5353.	7.1	26
65	Investigating the Interaction of Octapeptin A3 with Model Bacterial Membranes. ACS Infectious Diseases, 2017, 3, 606-619.	3.8	25
66	Tuning the activity of Cu-containing rare earth oxide catalysts for CO oxidation reaction: Cooling while heating paradigm in microwave-assisted synthesis. Materials Research Bulletin, 2018, 108, 142-150.	5.2	25
67	The αâ€importome of mammalian germ cell maturation provides novel insights for importin biology. FASEB Journal, 2014, 28, 3480-3493.	0.5	24
68	The Effect of Ni Addition onto a Cu-Based Ternary Support on the H2 Production over Glycerol Steam Reforming Reaction. Nanomaterials, 2018, 8, 931.	4.1	24
69	Electron spectroscopic studies of nanocomposite PVD TiAlBN coatings. Vacuum, 2002, 67, 471-476.	3.5	23
70	Ni Catalysts Based on Attapulgite for Hydrogen Production through the Glycerol Steam Reforming Reaction. Catalysts, 2019, 9, 650.	3.5	23
71	Investigation of the electrochemical behaviour and surface chemistry of a Tiâ€13Nbâ€13Zr alloy exposed in MEM cell culture media with and without the addition of H <sub>2</sub> O <sub>2</sub> . Surface and Interface Analysis, 2008, 40, 220-224.	1.8	21
72	Characterization of the metal–semiconductor interface of gold contacts on CdZnTe formed by electroless deposition. Journal Physics D: Applied Physics, 2015, 48, 275304.	2.8	21

#	Article	IF	CITATIONS
73	Proton irradiation of CdTe thin film photovoltaics deposited on ceriumâ€doped space glass. Progress in Photovoltaics: Research and Applications, 2017, 25, 1059-1067.	8.1	21
74	Development and characterisation of zinc oxalate conversion coatings on zinc. Corrosion Science, 2018, 137, 13-32.	6.6	21
75	Nanostructured Fe-Ni Sulfide: A Multifunctional Material for Energy Generation and Storage. Catalysts, 2019, 9, 597.	3.5	21
76	Continuous selective deoxygenation of palm oil for renewable diesel production over Ni catalysts supported on Al <sub>2</sub> O <sub>3</sub> and La <sub>2</sub> O <sub>3</sub> –Al <sub>2</sub> O <sub>3</sub> . RSC Advances, 2021, 11, 8569-8584.	3.6	21
77	Synthesis and properties of 1D Sm-doped CeO2 composite nanofibers fabricated using a coupled electrospinning and sol–gel methodology. Ceramics International, 2016, 42, 10734-10744.	4.8	20
78	Visible Light Water Splitting via Oxidized TiN Thin Films. Journal of Physical Chemistry C, 2012, 116, 15855-15866.	3.1	19
79	Surface characterisation and photocatalytic performance of N-doped TiO2 thin films deposited onto 200Ânm pore size alumina membranes by sol–gel methods. Materials Chemistry and Physics, 2015, 159, 25-37.	4.0	19
80	Sputum Active Polymyxin Lipopeptides: Activity against Cystic FibrosisPseudomonas aeruginosalsolates and Their Interactions with Sputum Biomolecules. ACS Infectious Diseases, 2018, 4, 646-655.	3.8	19
81	Effect of total gas pressure and O2/N2 flow rate on the nanostructure of N-doped TiO2 thin films deposited by reactive sputtering. Thin Solid Films, 2014, 552, 10-17.	1.8	17
82	Proteomic Profiling of Human Uterine Fibroids Reveals Upregulation of the Extracellular Matrix Protein Periostin. Endocrinology, 2018, 159, 1106-1118.	2.8	17
83	The flagellar protein Enkurin is required for mouse sperm motility and for transport through the female reproductive tractâ€. Biology of Reproduction, 2018, 99, 789-797.	2.7	17
84	Decoupling the Chemical and Mechanical Strain Effect on Steering the CO <sub>2</sub> Activation over CeO <sub>2</sub> -Based Oxides: An Experimental and DFT Approach. ACS Applied Materials & Interfaces, 2022, 14, 33094-33119.	8.0	17
85	Comparison of the surfaces and interfaces formed for sputter and electroless deposited gold contacts on CdZnTe. Applied Surface Science, 2018, 427, 1257-1270.	6.1	16
86	Hydrogen production via steam reforming of glycerol over Ce-La-Cu-O ternary oxide catalyst: An experimental and DFT study. Applied Surface Science, 2022, 586, 152798.	6.1	16
87	Comparison of Ar+ Monoatomic and Cluster Ion Sputtering of Ta2O5 at Different Ion Energies, by XPS: Part 2 - Cluster Ions. Surface Science Spectra, 2014, 21, 68-83.	1.3	15
88	Comparison of Ar+ Monoatomic and Cluster Ion Sputtering of Ta2O5 at Different Ion Energies, by XPS: Part 1 - Monoatomic Ions. Surface Science Spectra, 2014, 21, 50-67.	1.3	15
89	A Comparative Study of Outer Membrane Proteome between Paired Colistin-Susceptible and Extremely Colistin-Resistant <i>Klebsiella pneumoniae</i> Strains. ACS Infectious Diseases, 2018, 4, 1692-1704.	3.8	15
90	Remote plasma sputtering of indium tin oxide thin films for large area flexible electronics. Thin Solid Films, 2011, 520, 1207-1211.	1.8	14

#	Article	IF	CITATIONS
91	Ni <sub>2</sub> P Nanoparticles Embedded in Mesoporous SiO <sub>2</sub> for Catalytic Hydrogenation of SO <sub>2</sub> to Elemental S. ACS Applied Nano Materials, 2021, 4, 5665-5676.	5.0	14
92	Towards maximizing conversion of ethane and carbon dioxide into synthesis gas using highly stable Ni-perovskite catalysts. Journal of CO2 Utilization, 2022, 61, 102046.	6.8	14
93	Proteomic Analysis Reveals that Topoisomerase 2A is Associated with Defective Sperm Head Morphology. Molecular and Cellular Proteomics, 2020, 19, 444-455.	3.8	13
94	Establishing and maintaining fertility: the importance of cell cycle arrest. Genes and Development, 2021, 35, 619-634.	5.9	12
95	Characterization of MOCVD Thin-Film CdTe Photovoltaics on Space-Qualified Cover Glass. IEEE Journal of Photovoltaics, 2016, 6, 557-561.	2.5	11
96	Introduction to a series of dicarboxylic acids analyzed by x-ray photoelectron spectroscopy. Surface Science Spectra, 2017, 24, .	1.3	11
97	Nickel Phosphide Nanoparticles for Selective Hydrogenation of SO <sub>2</sub> to H <sub>2</sub> S. ACS Applied Nano Materials, 2021, 4, 6568-6582.	5.0	11
98	Investigation of sulphur diffusion at the CdS/CdTe interface of thin-film solar cells. Surface and Interface Analysis, 2002, 33, 825-829.	1.8	9
99	Quantitative Glycopeptide Changes in Rat Sperm During Epididymal Transit1. Biology of Reproduction, 2016, 94, 91.	2.7	9
100	Thin film cadmium telluride solar cells on ultraâ€thin glass in low earth orbit—3Âyears of performance data on the AlSatâ€1N CubeSat mission. Progress in Photovoltaics: Research and Applications, 2021, 29, 1000-1007.	8.1	9
101	Oxidative coupling of methane on Li/CeO2 based catalysts: Investigation of the effect of Mg- and La-doping of the CeO2 support. Molecular Catalysis, 2022, 520, 112157.	2.0	9
102	Performance comparison of small-pixel CdZnTe radiation detectors with gold contacts formed by sputter and electroless deposition. Journal of Instrumentation, 2017, 12, P06015-P06015.	1.2	8
103	Deposition and characterization of a sol-gel Mg-substituted fluorapatite coating with new stoichiometries. Applied Surface Science, 2020, 505, 144393.	6.1	8
104	The Plasma Protein Binding Proteome of Ertapenem: A Novel Compound-Centric Proteomic Approach for Elucidating Drug–Plasma Protein Binding Interactions. ACS Chemical Biology, 2016, 11, 3353-3364.	3.4	7
105	Nanostructural Characterisation and Optical Properties of Sputter-Deposited Thick Indium Tin Oxide (ITO) Coatings. Coatings, 2020, 10, 1127.	2.6	7
106	Molecular Characterisation of the Haemagglutinin Glycan-Binding Specificity of Egg-Adapted Vaccine Strains of the Pandemic 2009 H1N1 Swine Influenza A Virus. Molecules, 2015, 20, 10415-10434.	3.8	6
107	Lightweight and lowâ€cost thin film photovoltaics for large area extraâ€ŧerrestrial applications. IET Renewable Power Generation, 2015, 9, 420-423.	3.1	6
108	Oxidation of a depleted uraniumâ€5 wt% molybdenum (Uâ€5Mo) alloy in UHV by AES and XPS. Surface and Interface Analysis, 2019, 51, 849-856.	1.8	6

Mark A Baker

#	Article	IF	CITATIONS
109	Ni/CNT/Zeolite-Y composite catalyst for efficient heptane hydrocracking: Steady-state and transient kinetic studies. Applied Catalysis A: General, 2022, 630, 118437.	4.3	6
110	Ion-driven nanograin formation in early-stage degradation of tri-cation perovskite films. Nanoscale, 2022, 14, 2605-2616.	5.6	6
111	The adsorption of an epoxy acrylate resin on aluminium alloy conversion coatings. International Journal of Adhesion and Adhesives, 2011, 31, 687-694.	2.9	5
112	Dicarboxylic acids analysed by x-ray photoelectron spectroscopy, Part II - butanedioic acid anhydrous. Surface Science Spectra, 2017, 24, .	1.3	5
113	Dicarboxylic acids analysed by x-ray photoelectron spectroscopy, Part V - heptanedioic acid anhydrous. Surface Science Spectra, 2017, 24, 011105.	1.3	5
114	Modeling of Heat Transfer in an Aluminum X-Ray Anode Employing a Chemical Vapor Deposited Diamond Heat Spreader. Journal of Heat Transfer, 2018, 140, .	2.1	5
115	Carbon nanotube micro-contactors on ohmic substrates for on-chip microelectromechanical probing applications at wafer level. Carbon, 2019, 150, 117-127.	10.3	5
116	The Effect of Cracking of Thermally Grown Oxide Layers in Thermal Barrier Coatings Examined Using FIB Tomography and Inverse Modelling. Oxidation of Metals, 2021, 96, 157-168.	2.1	5
117	A study of the surface chemistry, morphology and wear of silicon based MEMS. Surface and Interface Analysis, 2004, 36, 1254-1258.	1.8	4
118	Dicarboxylic acids analysed by x-ray photoelectron spectroscopy, Part IV - hexanedioic acid anhydrous. Surface Science Spectra, 2017, 24, 011104.	1.3	4
119	Dicarboxylic acids analysed by x-ray photoelectron spectroscopy, Part VI - octanedioic acid anhydrous. Surface Science Spectra, 2017, 24, 011106.	1.3	4
120	Sialylation of Asparagine 612 Inhibits Aconitase Activity during Mouse Sperm Capacitation; a Possible Mechanism for the Switch from Oxidative Phosphorylation to Glycolysis. Molecular and Cellular Proteomics, 2020, 19, 1860-1875.	3.8	4
121	Dicarboxylic acids analysed by x-ray photoelectron spectroscopy, Part I - propanedioic acid anhydrous. Surface Science Spectra, 2017, 24, .	1.3	3
122	Dicarboxylic acids analysed by x-ray photoelectron spectroscopy, Part III - pentanedioic acid anhydrous. Surface Science Spectra, 2017, 24, 011103.	1.3	3
123	Contemporary Anti-Ebola Drug Discovery Approaches and Platforms. ACS Infectious Diseases, 2019, 5, 35-48.	3.8	3
124	Probing Nanoscale Schottky Barrier Characteristics at WSe <sub>2</sub> /Graphene Heterostructures via Electrostatic Doping. Advanced Electronic Materials, 0, , 2200196.	5.1	3
125	Quantitative atomic force microscopy: A statistical treatment of high-speed AFM data for quality control applications. Ultramicroscopy, 2022, 239, 113546.	1.9	3
126	Failure characteristics of adhesively bonded aluminium for spacecraft applications. Surface and Interface Analysis, 2008, 40, 132-136.	1.8	2

#	Article	IF	CITATIONS
127	Growth anomalies in CVD silicon carbide monofilaments for metal matrix composites. Materialia, 2021, 16, 101087.	2.7	2
128	Metal-Free Phosphated Mesoporous SiO2 as Catalyst for the Low-Temperature Conversion of SO2 to H2S in Hydrogen. Nanomaterials, 2021, 11, 2440.	4.1	1
129	Dicarboxylic acids analyzed by time-of-flight secondary ions mass spectrometry. Part II: Butanedioic acid. Surface Science Spectra, 2017, 24, 021403.	1.3	0

130 Dicarboxylic acids analyzed by time-of-flight secondary ion mass spectrometry (Introduction to parts) Tj ETQq0 0 0 rgBT /Overlock 10 Tf

131	Dicarboxylic acids analyzed by time-of-flight secondary ion mass spectrometry. Part 0: Ethanedioic acid. Surface Science Spectra, 2017, 24, 021401.	1.3	0
132	Dicarboxylic acids analyzed by time-of-flight secondary ions mass spectrometry. Part I: Propanedioic acid. Surface Science Spectra, 2017, 24, 021402.	1.3	0
133	Dicarboxylic acids analyzed by time-of-flight secondary ions mass spectrometry. Part III: Pentanedioic acid. Surface Science Spectra, 2017, 24, 021404.	1.3	0
134	Dicarboxylic acids analyzed by time-of-flight secondary ions mass spectrometry. Part IV: Hexanedioic acid. Surface Science Spectra, 2017, 24, 021405.	1.3	0
135	Dicarboxylic acids analyzed by time-of-flight secondary ions mass spectrometry. Part V: Heptanedioic acid. Surface Science Spectra, 2017, 24, 021406.	1.3	0
136	Dicarboxylic acids analyzed by time-of-flight secondary ions mass spectrometry. Part VI: Oxanedioic acid. Surface Science Spectra, 2017, 24, 021407.	1.3	0
137	Official Call: 2018 Annual Business Meeting of the American Osteopathic Association. Journal of Osteopathic Medicine, 2018, 118, 433-433.	0.8	0
138	DNA variants are an unlikely explanation for the changing quality of spermatozoa within the same individual. Human Fertility, 2021, 24, 376-388.	1.7	0
139	Extending XPS Surface Analysis with Correlative Spectroscopy and Microscopy. Microscopy and Microanalysis, 2020, 26, 1016-1016.	0.4	0
140	Phosphoproteomic Analysis of Peptides. Methods in Molecular Biology, 2013, 1069, 271-277.	0.9	0